Journal Name

ARTICLE

Zinc(II), cobalt(II) and manganese(II) networks with phosphoserine ligand: Synthesis, crystal structures magnetic and conduction properties

Received 00th January 20xx,
Accepted 00th January 20xx

DOI: 10.1039/x0xx00000x

www.rsc.org/

J. Vallejo,[a] I. R. Salcedo,[b] R. M. P. Colodrero,[b] A. Cabeza,[b] A. Świtlicka,[c] J. Cano[a] and M. Viciano-Chumillas[a,*]

A series of zinc(II), cobalt(II) and manganese(II) coordination networks with the phosphoserine ligand (Pser) is synthesized and characterized. Whereas in compounds **1** and **2** with the general formula $[M(Pser)]_n$ [M = Zn (**1**) and Co(**2**)], the metal(II) ion presents a tetrahedral geometry, in $[Co(Pser)(H_2O)_2]_n$ (**3**) and $[Mn(Pser)(H_2O)]_n$ (**4**)], the metal(II) ions are in a distorted octahedral geometry. The 3D frameworks are formed by inorganic layers built up from MO_4 or MO_6 polyhedra and phosphate groups. These layers are linked by the carboxylate groups of the phosphoserine ligand. The presence of extended hydrogen bonding stabilizes the 3D network and favors the proton transfer leading to moderate proton conductors. The highest proton conductivity, 2.70×10^{-5} S cm^{-1} (at 80 ºC and 95% RH), is obtained for compound **3**. Temperature dependent magnetic susceptibility measurements for **2**–**4** reveal predominant antiferromagnetic interactions between the paramagnetic metal(II) ions.

Introduction

In the last decades, metal-organic frameworks (MOFs) or porous coordination polymers (PCPs) have received enormous attention as a result of different applications in gas storage,[1] molecular separation,[2] catalysis,[3] optics[4,5] and biomedicine.[6,7] MOFs are generally formed by metal ions or metal clusters and organic ligands.[8] Carboxylate ligands are the most exploited organic ligands. Nevertheless, phosphonate ligands have recently become an alternative to them and the interest of metal phosphonates have grown considerably.[9–12] This fact is due to the additional coordination site that the phosphonic group possesses, increasing the number of coordination modes as compared with the carboxylic acid ligands. Furthermore, phosphonate groups form stronger bonds than carboxylates. Then, the coordination compounds display higher thermal and chemical stabilities. On the other hand, the main problem of the phosphonate ligands resides in the lower crystallinity of the final products as compared to the carboxylate ligands. Hence, a successful synthetic strategy consists on the employ of a combination of both functionalities in the same ligand.

On the other hand, aminoacids are biologically important molecules with amino and carboxylic groups. They are promising ligands for the design of bio-inspired metal organic frameworks (BioMOFs),[13] because of their flexibility and also of the zwitterion, which can induce interesting properties, such as gas and magnetic data storage, sensors, etc.[12,14] Another property not so exploited in coordination polymers is proton conductivity with applications in transport dynamics, electrochemical devices and fuel cells.[12,15–17] The main requirements for a MOF material to be proton conductive are the presence of acidic groups that can be proton-carrier sources, and hydrogen bonded networks that can be proton conduction pathways.

Our approach is to employ the phosphoserine ligand (Scheme 1), which is the phosphate derivative of the serine aminoacid. In this work, different transition-metal ions, *i.e.* cobalt(II), manganese(II) and zinc(II) are investigated for the formation of new coordination networks with the phosphoserine ligand (Pser). To the best of our knowledge, only three polymorphic forms of potassium salt[18] and a copper complex[19] based on the phosphoserine ligand have been reported in the Cambridge Structural Database (CSD).[20] As result of our work, the synthesis, characterization and crystal structures of four new

[a] *Institut de Ciència Molecular (ICMol), Universitat de València, 46980 Paterna, València*
[b] *Departamento de Química Inorgánica, Cristalografía y Mineralogía, Universidad de Málaga, Campus de Teatinos s/n, Málaga-29071, Spain*
[c] *Department of Crystallography, Institute of Chemistry, University of Silesia, 9th Szkolna St., 40-006 Katowice, Poland*

Electronic Supplementary Information (ESI) available: Rietveld plot, X-ray powder diffraction patterns, view of the hydrogen bonding, thermogravimetric analysis, impedance measurements, field-dependence of the magnetization plot and magnetic network representations. See DOI: 10.1039/x0xx00000x

compounds are reported: $[M(Pser)]_n$ [M = Zn(II) (**1**), Co(II) (**2**)], $[Co(Pser)(H_2O)_2]_n$ (**3**) and $[Mn(Pser)(H_2O)]_n$ (**4**)]. Furthermore, their magnetic and proton conduction properties are described.

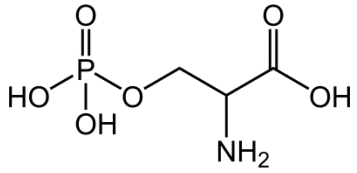

Scheme 1. Phosphoserine (PSer).

Experimental Section

Materials. All chemicals were obtained from commercial sources and used as received.

Syntheses.

$[Zn(PSer)]_n$ (**1**). $ZnCl_2$ (68 mg, 0.5 mmol) and Pser (92 mg, 0.5 mmol) were dissolved in a H_2O:DMF mixture with a ratio of 1:0.06 (40 mL) in a scintillation vial. The vial was heated at 85ºC during 6 h. White crystals were found and collected by filtration. Yield: 113 mg (91%). Anal. Calcd for **1** ($C_3H_6NO_6PZn$): C, 14.50; H, 2.43; N, 5.64. Found: C, 14.54; H, 2.08; N, 5.84. IR (ν_{max}/cm^{-1}): 3446(br), 3165(m), 1652(s), 1612(s), 1545(m), 1488(s), 1428(m), 1391(w), 1359(w), 1261(w), 1177(s), 1158(s), 1123(s), 1087(s), 1007(s), 981(m), 930(w), 883(m), 839(s), 701(m), 575(m), 547(m).

$[Co(PSer)]_n$ (**2**). $CoCl_2{\cdot}6H_2O$ (47 mg, 0.2 mmol) and PSer (37 mg, 0.2 mmol) in H_2O:EtOH mixture with a 1:5 ratio, were loaded into a scintillation vial. The vial was heated at 85 ºC for 8 h. Blue crystals were found and collected by filtration. Yield: 28 mg (57%). Anal. Calcd for **2** ($C_3H_6NO_6PCo$): C, 14.89; H, 2.50; N, 5.79. Found: C, 14.83; H, 1.91; N, 5.62. IR (ν_{max}/cm^{-1}): 3428(br), 3159(m), 1648(s), 1637(s), 1611(s), 1540(m), 1490(s), 1428(m), 1391(w), 1359(w), 1258(w), 1177(s), 1155(s), 1105(s), 1085(s), 1004(s), 983(m), 926(w), 881(m), 837(s), 707(m), 577(m), 548(m).

$[Co(PSer)(H_2O)_2]_n$ (**3**). $CoCl_2{\cdot}6H_2O$ (95 mg, 0.4 mmol) and PSer (74 mg, 0.4 mmol) in H_2O:EtOH in a 1:1 ratio were loaded into a scintillation vial. Then, triethylamine (80 μl) was added to adjust the pH around 4.5. The vial was heated at 90 ºC for 56 h. Small pink crystals were found and collected by filtration. Yield: 82 mg (75%). Anal. Calcd for **3** ($C_3H_{10}NO_8PCo$): C, 12.96; H, 3.63; N, 5.04. Found: C, 12.69; H, 3.26; N, 5.24. IR (ν_{max}/cm^{-1}): 3620(m), 3422(br), 3135(w), 1624(s), 1575(s), 1492(s), 1466(s), 1401(s), 1371(w), 1356(m), 1299(m), 1252(w), 1153(s), 1103(s), 1078(s), 1024(s), 997(s), 897(m), 827(w), 770(m), 631(m), 531(m).

$[Mn(PSer)(H_2O)]_n$ (**4**). $Mn(OAc)_2{\cdot}4H_2O$ (122 mg, 0.5 mmol) and PSer (92 mg, 0.5 mmol) in H_2O:MeCN in a 2:1 ratio were heated into a scintillation vial at 85ºC during 56 h. White crystals were found and collected by filtration. Yield: 115 mg (90%). Anal. Calcd for **4** ($C_3H_8MnNO_7P$): C, 14.07; H, 3.15; N, 5.47. Found: C, 13.86; H, 3.51; N, 5.35. IR (ν_{max}/cm^{-1}): 3246(m), 3212(m), 1662(s), 1611(s), 1577(s), 1516(m), 1454(s), 1403(m), 1376(s), 1317(m), 1272(m), 1127(s), 1077(s), 1052(s), 997(s), 962(s), 891(m), 791(s), 708(s), 589(s), 526(s).

Physical Techniques. Infrared spectra (4000–500 cm^{-1}) were recorded on a Nicolet 5700 spectrophotometer as KBr pellets. Elemental analyses (C, H, N) were performed at the Servei Central de Suport a la Investigació (SCSIE) from the Universitat de València (Spain). X-Ray Powder diffraction data were collected with an Empyrean PANalytical powder diffractometer in Bragg-Brentano configuration using Cu Kα radiation. Thermodiffractometric studies for **3** were carried out on a PANanalytical X'Pert Pro diffractometer (Cu $K\alpha_1$) using an Anton Paar TTK450 Camera under static air. Before recording any pattern, the sample was hold at each temperature for 15 min allowing any structural transformation. For the structural determination of compound **4**, powder diffraction pattern was collected on a D8 ADVANCE (Bruker AXS) diffractometer, in transmission configuration, equipped with a Johansson Ge(111) primary monochromator (Mo $K\alpha_1$, λ = 0.7093 Å) and a LYNXEYE XE detector. The XRPD pattern was recorded between 3 and 80º (2θ), 0.01º step size and an equivalent counting time of ca. 1536 s/step.

Magnetic Measurements. Variable-temperature (2–300 K) direct current (dc) magnetic susceptibility measurements under an applied field of 0.25 (T < 30 K) and 5.0 kG (T ≥ 30 K), and variable-field (0.0–5.0 T) magnetization measurements at 2.0 K were carried out with a Quantum Design SQUID magnetometer on powdered single-crystals restrained with eicosane.

Theoretical calculations. DFT calculations were performed on models built from extended networks of compounds **2** and **3** through the Gaussian 09 package using the B3LYP functional,[21] the quadratic convergence approach and a guess function generated with the fragment tool of the same program.[22] Triple- and double-ζ quality basis sets proposed by Ahlrichs and co-workers are employed for the metal and non-metal atoms, respectively.[23] Solvation effects (acetonitrile solvent) were considered through a polarizable continuum model (PCM) where the cavity is created via a series of overlapping spheres.[24,25] The magnetic coupling states were obtained from the relative energies of the broken-symmetry (BS) singlet spin state from the high-spin state with parallel local spin moments.[26,27] In order to evaluate the axial zero-field splitting (*D*), calculations based on a wave function obtained from a complete active space (CAS) calculation were performed with version 3.0 of the ORCA programme,[28] using the TZVP basis set proposed by Ahlrichs[23] and the auxiliary TZV/C Coulomb fitting basis sets.[29,30]

Proton Conductivity Studies. Electrical characterization for compounds **1**, **3** and **4** was carried out on dense (~96%–98% theoretical density) cylindrical pellets (diameter *ca*. 5 mm and thickness *ca*. 1 mm) obtained by pressing *ca*. 40 mg of sample at 250 MPa, for 1 min. The pellets were pressed between porous C electrodes (Sigracet, No. GDL 10 BB, no Pt). The sample cell was placed inside a temperature- and humidity-controlled chamber (Espec, Model SH-222) and connected to an impedance analyzer (Agilent, Model HP4284A). AC impedance data were collected over the frequency range from

20 Hz to 1 MHz with an applied voltage of 1 V. To equilibrate water content, pellets were first preheated (0.2 °C/min) from 25 to 80 °C and RH 95%. Proton conductivity measurements were recorded on cooling using a stabilization time of 3−5 h for each temperature (80, 70, 60, 50, 40, 30 and 25 °C). Water condensation on sample was avoided by reducing first the relative humidity before decreasing temperature. All measurements were electronically controlled by the winDETA package of programs.[31]

X-ray Crystallography. Single-crystal X-ray diffraction data of **1**–**3** were collected on a Gemini A Ultra diffractometer equipped with an Atlas CCD detector and graphite monochromated MoKα radiation (λ = 0.71073 Å) at room temperature. The unit cell determination and data integration were carried out using the CrysAlis package of Oxford Diffraction.[32] Lorentz, polarization and empirical absorption corrections using spherical harmonics implemented in the SCALE3 ABSPACK scaling algorithm were applied.[17] The structures were solved by direct methods using SHELXS97 and refined by full-matrix least-squares on F2 using SHELXL97.[33] All non-hydrogen atoms were refined with anisotropic displacement parameters. For compound **4**, powder pattern indexing, space group determination, and structure determination were carried out using the program EXPO2014.[34] The crystal structure was solved by default using a simulated annealing approach with the crystal structure of **3** as starting model. The best solution showed all the atomic positions. The final model was obtained by Rietveld refinement[35] using the GSAS package.[36,37] In order to maintain chemically reasonable geometry for the phosphoserine ligand the following soft constraints were used: P−O [1.53(1) Å], C−O [1.45(1) Å], O···O [2.55(2) Å], C−C [1.50(1) Å], C−N [1.50(1) Å], C−O_{carb} [1.23(1) Å], O_{carb}···O_{carb} [2.21(2) Å] and C···O_{carb} [2.38(2) Å], C···N [2.46(2) Å], P···C [2.88(2) Å]. The final weight for the soft constraints was 7. No attempts to locate the H atoms were carried out due to the limited quality of the XRPD data. A common isotropic atomic displacement parameter was refined, one for the manganese atom, a second one for the phosphorous atom and a third for the remaining atoms (C, N and O). The final Rietveld plot is shown in Figure S1. Details of the crystallographic data collection, structural determination, and refinement for **1–4** are given in Table 1. Crystallographic data for the structures reported in this paper have been deposited with the Cambridge Crystallographic Data Centre as supplementary publication CCDC–1567558 (**1**), 1567559 (**2**), 1567557 (**3**) and 1563742 (**4**). Copies of the data can be obtained free of charge on application to CCDC, 12 Union Road, Cambridge CB21EZ, UK (fax: (+44) 1223-336-033; e-mail: deposit@ccdc.cam.ac.uk).

Results and discussion

Syntheses and characterization. The reaction of $ZnCl_2$ and PSer in a water:dimethylformamide mixture affords compound **1**. Compound **1** is also obtained by employing different zinc(II) salts ($Zn(OAc)_2{\cdot}2H_2O$, $Zn(NO_3)_2{\cdot}6H_2O$, *etc*) and in a ratio metal to ligand 1:1 and 1:2. The product can also be obtained by heating under reflux. However, better crystals are achieved under solvothermal conditions employing scintillation vials. Compounds **2** and **3** are obtained by solvothermal reaction of Pser and $CoCl_2{\cdot}6H_2O$. The reaction time, the type of solvents and their ratio, and the pH are crucial to determine the final compound. Low pH values, together with short reaction times and water/ethanol or water/acetone mixtures with large organic solvent ratio favour compound **2**, whereas higher pH, longer reaction times, water/acetonitrile mixtures with larger water ratio prompt the formation of compound **3**. The reaction of a manganese(II) salt, such as $MnCl_2{\cdot}4H_2O$ or $Mn(OAc)_2{\cdot}4H_2O$ with PSer in water/methanol or water/acetonitrile affords compound **4**.

The infrared spectra of **1**–**4** show the absence of the bands of the carboxylic acid group at 1797 cm^{-1} and the phosphoric acid at 2698 cm^{-1}, suggesting that both acids are deprotonated and that the ligand coordinates to the metal(II) ions. In **1**–**4**, strong bands are present between 1177 and 997 cm^{-1}, typical from the P−OR and P=O vibrations. In **1**–**3**, the sharp band at ~ 3165 cm^{-1} belongs to the ν_{NH3} stretching form, whereas in **4**, two sharp bands appear at 3246 and 3212 cm^{-1}, probably due to the different hydrogen bonding network. In addition, in compounds **3**, a sharp band at 3620 cm^{-1} indicates the presence of coordinated water molecules, which is absence in compound **2**.

Description of the Molecular Structures. Powder X-ray diffraction (XRPD) studies reveal a well match between the patterns simulated from the single-crystal X-ray and the experimental data for compounds **1**–**3** (Figure S2). The crystal structure resolution of compound **4** was solved from laboratory powder diffraction pattern using Mo $K_{\alpha 1}$ radiation (see experimental section).

Crystallographic data for compound **1**–**4** are given in Table 1. Compounds **1** and **2**, which are isostructural, crystallize in the orthorhombic $P2_12_12_1$ (no. 19) space group. Their structures consist of a 3D network built by asymmetric units of one phosphoserine ligand coordinated to the zinc(II) and cobalt(II) ions in **1** and **2**, respectively (Figures 1 and S3). The phosphoserine ligand has the two acid groups deprotonated, whereas the amino group is protonated. The existence of zwitterions is common for phosphonic acids[12] with amine groups and also for aminoacids. In both cases, the metal(II) ion has a distorted tetrahedral geometry formed by three oxygen atoms from three different phosphate ligands and one oxygen from a carboxylate ligand. The other oxygen atom from this carboxylate group remains uncoordinated. Selected bond distances and angles are listed in Table 2. The M−O distances are in the range of 1.910(3)−1.984(3) Å and 1.934(4)−1.994(4) Å for **1** and **2**, respectively. The O−M−O angles are between 101.93(15) and 119.42(13)º for **1** and 101.38(17) and 120.13(15)º for **2**, being both in all cases different from an ideal tetrahedron. The P−O distances are in the range of 1.503(4)−1.606(3) Å and 1.506(4)−1.611(4) Å for **1** and **2**, respectively. Each PO_4 tetrahedron is bonded to three different metal(II) ion and to the organic ligand. As a result, the three-dimensional structure can be described as pillared solids where the organic ligand acts as a pillar between the inorganic

layers formed by the phosphate and MO_4 tetrahedron in the *b* direction (Figure 2). The shortest M···M distances are 5.099 Å for **1** and 5.202 Å for **2**.

Table 1. Crystal data for compounds **1**–**4**.

	1	**2**	**3**	**4**
Formula	$C_3H_6ZnNO_6P$	$C_3H_6CoNO_6P$	$C_3H_{10}CoNO_8P$	$C_3H_8MnNO_7P$
Formula weight [gmol^{-1}]	248.45	241.99	278.02	256.01
Crystal system	Orthorrombic (no19)	Orthorrombic (no19)	Monoclinic	Monoclinic
Space group	$P2_12_12_1$	$P2_12_12_1$	$P2_1$	$P2_1$
a [Å]	5.1818(6)	5.202(4)	5.4432(4)	5.6064(11)
b [Å]	7.6909(9)	7.7413(4)	9.9568(7)	12.4389(2)
c [Å]	17.7166(15)	17.7009(13)	7.6434(7)	75.3710(10)
α [º]	90	90	90	90
β [º]	90	90	98.030(8)	105.7562(10)
γ [º]	90	90	90	90
V [Å^3]	706.05(13)	712.8(6)	409.73(6)	360.49(12)
Z	4	4	2	2
Dcalc [gcm^{-3}]	1.325	2.255	2.253	2.284
Number of collected reflections (unique)	2462(1248)	2931(1168)	1721(1128)	–
Number of observed reflections ($I_o > 2\sigma(I_o)$)	1132	1047	1067	–
Internal R factor	0.042	0.038	0.031	–
Number of parameters	110	110	130	–
Goodness-of-fit S on F^2	1.05	1.06	1.018	1.74
Largest peak and hole in final difference Fourier map (e Å^{-3})	–0.45 and 0.46	–0.40 and 0.50	–0.43 and 0.32	–
μ [mm^{-1}]	2.337	2.622	2.314	1.983
R_1[a] [$I > 2.0\sigma(I)$]	0.0335	0.0296	0.0307	–
wR_2[b] [all data]	0.0667	0.0637	0.0635	–
R_{wp}				6.54
R_P				5.14
R_F				2.02
T [K]	293	293	293	298

[a] $R_1 = \sum||F_o| - |F_c|| / \sum|F_o|$. [b] $wR_2 = \{\sum[w(F_o^2 - F_c^2)^2]/\sum w(F_o^2)^2\}^{1/2}$.

In addition, the three-dimensional network is stabilized by hydrogen bonding, which is present between the ammonium group and the carboxylate and phosphate groups of different ligands (Table 3 and Figure S4). Two types of porous are present in the network (Figures S4). The smallest one with the ammonium group pointed to the outer porous is *ca.* 8.462 Å and 8.493 Å (P···P distances) for **1** and **2**, respectively. The other channel is bigger with a porous of *ca.* 12.195 Å (**1**) and 12.236 Å (**2**) (P···P distances) in which the ammonium groups are in the inner space.

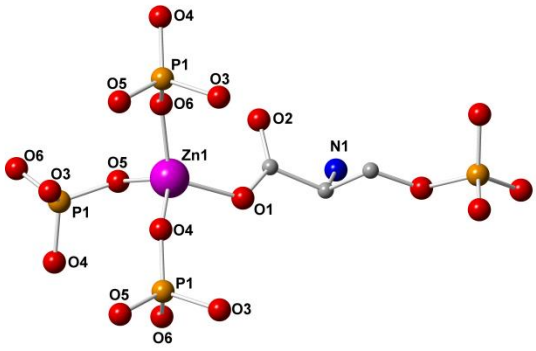

Figure 1. Tetrahedral coordination of Zn(II) ion and connectivity of the phosphoserine ligand in the crystal structure of $[Zn(Pser)]_n$ (**1**). Color code: magenta, zinc; orange, phosphorous; blue, nitrogen; red, oxygen; grey, carbon.

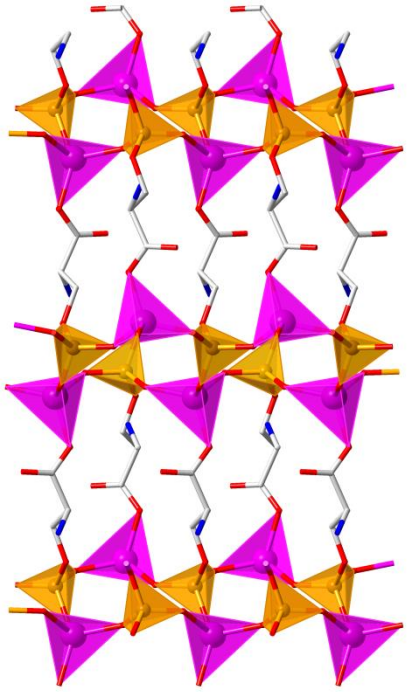

Figure 2. View of the 3-D network of **1** in the *b*-axis direction. Color code: magenta, zinc; orange, phosphorous; blue, nitrogen; red, oxygen; grey, carbon.

Table 2. Selected bond distances and angles for **1**–**4**.

	1	2	3	4
Bond distances				
M1–O1	1.967(4)	1.974(4)	2.044(5)	2.151(5)
M1–O2			2.026(5)	2.180(5)
M1–O3			2.139(5)	2.172(5)
M1–O4	1.924(4)	1.994(4)	2.002(5)	
M1–O5	1.984(4)	1.949(4)		2.182(6)
M1–O6	1.910(4)	1.934(4)	2.073(4)	2.259(5)
M1–O7			2.379(5)	
M1–Ow				2.356(7)
P1–O1				1.533(4)
P1–O2			1.495(5)	1.525(4)
P1–O3	1.606(4)	1.611(4)		1.534(4)
P1–O4	1.503(4)	1.515(4)	1.519(5)	1.633(4)
P1–O5	1.522(4)	1.508(4)	1.616(4)	
P1–O6	1.511(4)	1.506(4)	1.524(4)	
Bond angles				
O6–M1–O5	102.02(13)	110.22(16)		
O1–M1–O5	106.70(14)	101.38(17)	-	
O1–M1–O6			87.20(19)	87.9(3)
O1–M1–Ow				175.4(3)
O1–M1–O2			174.7(2)	
O1–M1–O3			92.2(2)	
O2–P1–O3				108.0(3)
O2–P1–O4			113.2(3)	107.8(4)
O2–P1–O5			104.3(3)	
O2–P1–O6			114.3(3)	
O3–P1–O4	109.05(18)	101.84(19)		109.2(4)
O3–P1–O5	101.98(17)	108.5(2)		
O3–P1–O6	107.74(17)	108.1(2)		
O4–P1–O5	111.51(19)	111.4(2)	107.6(3)	
O4–P1–O6	111.54(18)	114.8(2)	110.1(3)	
O5–P1–O6	114.41(18)	111.5(2)	106.7(3)	
M1–O4–P1	132.2(2)	119.88(19)	144.4(3)	
P1–O5–M1	120.46(17)	132.0(2)		
P1–O6–M1	131.6(2)	132.2(2)	134.1(3)	
O1–C1–O2	127.3(4)	127.5(5)		
O7–C3–O8			128.0(6)	

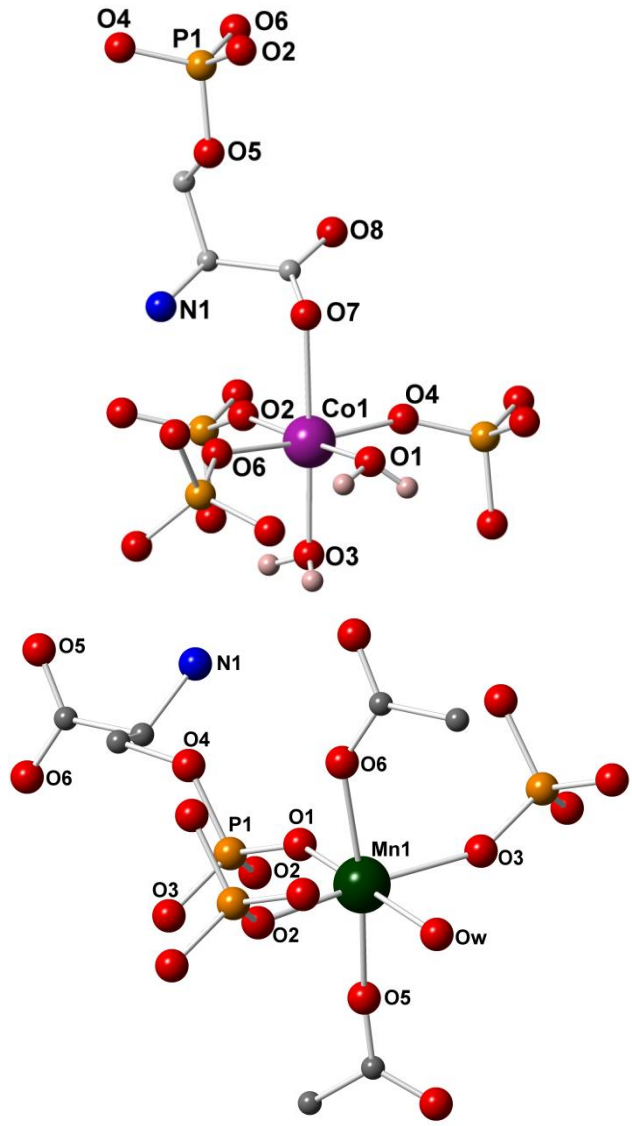

Figure 3. View of the coordination metal(II) ion sphere and the phosphoserine ligand in $[Co(Pser)(H_2O)_2]_n$ (**3**) (top) and $[Mn(Pser)(H_2O)]_n$ (**4**) (bottom). Color code: magenta, cobalt; green, manganese; orange, phosphorous; blue, nitrogen; red, oxygen; grey, carbon; pink, hydrogen.

Compound **3** crystallizes in the monoclinic $P2_1$ space group. Structure analysis reveals a three-dimensional network with a unit formed by a cobalt(II) ion, a phosphoserine ligand with deprotonated carboxylic and phosphoric acids, and two coordinated water molecules (Figure 3). As in compounds **1** and **2**, the amino group is protonated. Whereas in **2**, the cobalt(II) ion displays a distorted tetrahedral geometry, in **3**, the cobalt(II) ion presents a distorted axially elongated octahedral geometry, due to the two additional water molecules. The equatorial plane is formed by four oxygen atoms from three phosphoserine ligands and from one water molecule; whereas the axial positions are occupied by one water molecule and one carboxylic oxygen of a phosphoserine ligand. Selected bond distances and angles are listed in Table 2. The average Co–O distances are 2.0198 (eq) and 2.259 (ax) Å and the P–O distances are in the range of 1.497(4)–1.619(17) Å.

The shortest Co···Co distance is 5.251 Å. As for compounds **1** and **2**, the connectivity between the CoO_6 octahedra and PO_4 tetrahedra, and the phosphoserine ligands is preserved. Thus, the phosphoserine ligand acts as pillar between the inorganic layers formed from PO_4 and CoO_6 polyhedra (Figure 4) in the three-dimensional network. Hydrogen bonds between the phosphoserine ligand (ammonium, carboxylate and phosphate groups) and the coordinated water molecules stabilize the network (Table 3 and Figure S5).

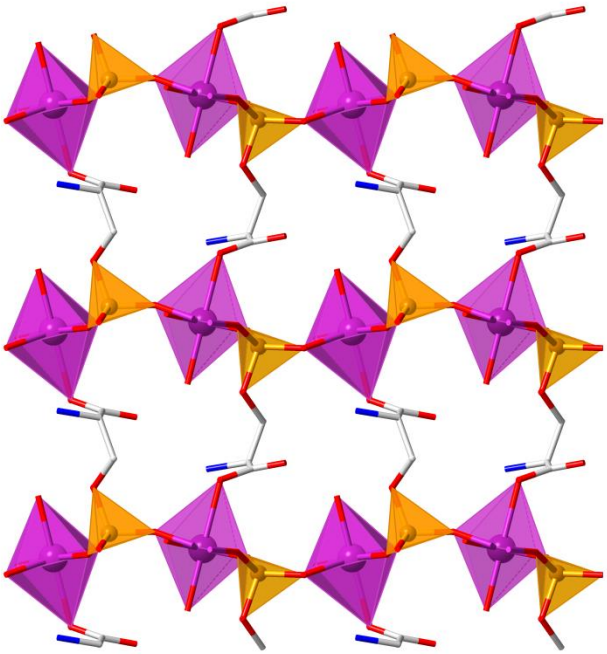

Figure 4. View of the 3-D network of **3** in the *a*-axis direction. Color code: magenta, cobalt; yellow, phosphorous; blue, nitrogen; red, oxygen; grey, carbon.

Compound **4** crystallizes in the monoclinic $P2_1$ space group. The structure consists of a manganese(II) ion with a phophoserine ligand and only one coordinated water molecules (Figure 3). The phosphoserine ligand has the two deprotonated acid functions, namely phosphoric and carboxylic acids. To balance the charge of **4**, the amino group should be protonated, as found in the previous compounds. The manganese(II) ion presents an axial distorted octahedral geometry. However, the coordination sphere is different from **3**. In **4**, the equatorial plane is formed by four oxygen atoms from four phosphoserine ligands, being two of the phosphate group and two of the carboxylate group, and the axial positions are filled by one water molecule and one phosphate oxygen of a phosphoserine ligand. Moreover, the coordination mode of the carboxylate group in **3** and **4** is different. Whereas in **3** the carboxylate ligand is monodentate, in **4** the carboxylate group acts as a bis-monodentate bridging ligand of two metal ions. Selected bond distances and angles are listed in Table 2. The average Mn–O_{eq} bond lengths is 2.198 Å and the Mn–O_{ax} distances are 2.150 (Mn–O1) and 2.356 Å (Mn–Ow). P–O bond lengths are in the range of 1.525(6)–1.634(5) Å. The shortest Mn···Mn distance is 5.371 Å. The three-dimensional framework can be described as pillared layer structure with inorganic layers (*ac*-plane) built up from MnO_6 octahedra and phosphate groups sharing vertexes (Figure 5). These layers are interconnected not only through the opposite sides of the phosphoserine ligand as in **1**–**3**, also through the carboxylate group. Thus, it leads to a more corrugated configuration of the phosphoserine ligand in the interlamellar region than for compounds **1**–**3**.

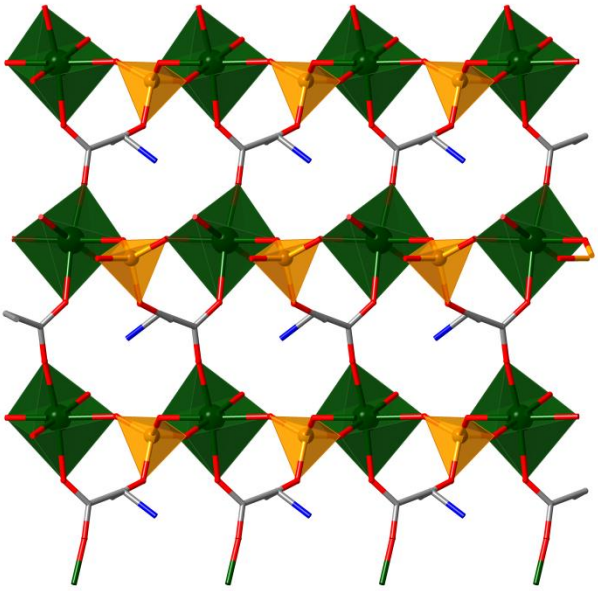

Figure 5. View of the 3-D network of **4** in the *c*-axis direction. Color code: green, manganese; yellow, phosphorous; blue, nitrogen; red, oxygen; grey, carbon.

Table 3. Hydrogen bonds details (distances [Å] and angles[º]) for **1**–**4**.

Donor–H···Acceptor	D–H	H···A	D···A	D–H···A
Compound **1**				
N1–H1A···O3intra	0.89	2.46	2.759(5)	100
N1–H1A···O4intra	0.89	2.27	2.937(5)	131
N1–H1A···O5	0.89	2.47	3.098(5)	128
N1–H1B···O5intra	0.89	2.15	2.922(5)	144
N1–H1C···O2	0.89	1.92	2.728(5)	150
Compound **2**				
N1–H1A···O3intra	0.89	2.45	2.763(5)	101
N1–H1A···O4intra	0.89	2.48	3.089(6)	126
N1–H1A···O5intra	0.89	2.27	2.927(6)	131
N1–H1B···O4intra	0.89	2.15	2.923(6)	144
N1–H1C···O2	0.89	1.93	2.732(6)	149
Compound **3**				
O1–H1A···O6	0.85	2.30	2.680(7)	107
O1–H1B···O4intra	0.85	1.76	2.588(7)	163
N1–H1C···O8	0.89	2.15	2.935(8)	147
N1–H1D···O2	0.89	2.51	3.068(7)	121
N1–H1D···O7intra	0.89	2.36	2.668(7)	100
N1–H1D···O6	0.89	2.16	3.026(7)	163
N1–H1E···O7intra	0.89	2.01	2.889(7)	168
O3–H3A···O5intra	0.85	2.50	3.143(7)	133
O3–H3B···O8	0.85	2.03	2.726(7)	139
Compound **4**				
N1···O3			2.866(9)	
N1···O4intra			2.958(9)	
N1···O4			3.020(8)	
N1···O5intra			2.702(9)	
N1···O5			3.122(8)	
N1···O6intra			2.653(8)	
N1···Ow			2.992(8)	
Ow···O1intra			2.920(7)	
Ow···O2			2.764(7)	
Ow···O3			3.024(9)	

Thermal and proton conduction studies. Previously to proton conductivity measurements, the thermal and water stability of solids were investigated. The TGA curves (Figure S6) show non mass loss below *ca.* 300 (**1**), 250 (**2**), 180 ºC (**3**) and 215 ºC (**4**), which indicate the stability of the networks and the strong coordination of the water molecules to the metallic centre, in case of the hydrated phases. Furthermore, the structural stabilities of compounds **1**–**4**, were also verified after exposure at high relative humidity (95%) by TGA and XRPD measurements. Whereas compounds **1**, **3** and **4** do not show changes in their TGA curves and XRPD patterns under these conditions, **2** transformed into **3** at high relative humidity and 80 ºC (Figures S7 and S8). This behaviour is expected since the solvatochromic equilibrium of the cobalt(II) ion is well-known.[38] However, the reversible dehydration of **3** to **2** was not observed by thermodiffraction (not shown).

In view of the hydrogen-bonded interactions between the different functional groups and water molecules, in the hydrated compounds, the proton conducting behaviours of **1**, **3** and **4** were studied. Impedance measurements were carried out between 25 and 80 ºC at 95 % RH. The overall pellet conductivities, determined from the semicircles in the Nyquist plots (Figure S9), are given in Figure 6 in a traditional Arrhenius plot. The highest proton conductivity measured at 80 ºC, 2.70×10^{-5} S cm^{-1}, was obtained for compound **3**. In it, the presence of two water molecules bonded to the metal cation, together with the ammonium ion and the carboxylate and phosphate groups, allows the creation of a more extended hydrogen-bond network than for the other members of the series. This value is in agreement with the reported for other metal polyphosphonates containing protonated N atoms as zwitterions.[39–42] As it is characteristic of many water-mediated proton conductors, a reduction on the relative humidity (data not shown) led to significant reduction in the proton conductivity. A partial or full elimination of the water content, in **4** and **1**, respectively, provoked a drop in the proton conductivity values of approximately an order of magnitude (7.17×10^{-6} S cm^{-1} (**4**) and 6.47×10^{-6} S cm^{-1} (**1**) at 80 ºC and 95% RH). The activation energies shown by all these solids are ranged between 0.30 and 0.40 eV, what suggests that the hydrogen-bonded arrays present in these solids constitute favourable proton transport pathways according to a Grotthuss mechanism (< 0.5 eV).[43,16]

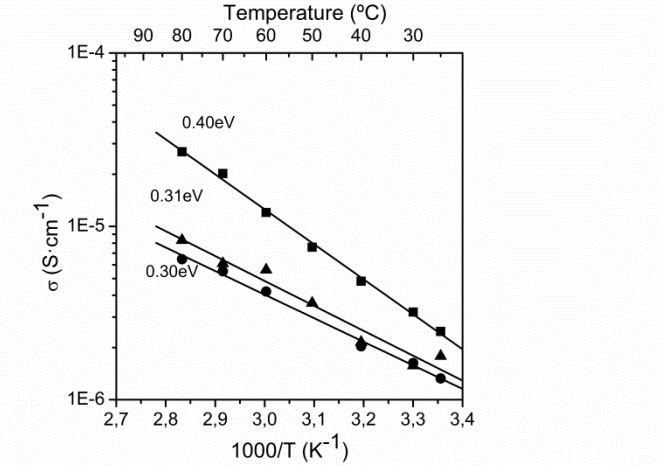

Figure 6. Arrhenius plots for compounds **1** (●), **3** (■) and **4** (▲).

Magnetic properties. Magnetic susceptibilities were measured under 0.5 T field in the 2–300 K temperature range for compounds **2**–**4**, as seen in Figure 7. The χ_MT values of **2** and **3** are 2.83 and 3.25 cm^{3}Kmol^{-1}, respectively, which are higher than the expected for an isotropic S = 3/2 spin moment with g = 2.0 (χ_MT = 1.875 cm^{3}Kmol^{-1}). These high values observed in **2** and **3** are usual in Co(II) ions that show a significant spin-orbit coupling (SOC). When lowering the temperature, the χ_MT product of both **2** and **3** decreases gradually until 50 K by the presence of SOC, but the expected limit value (χ_MT = 1.875 cm^{3}Kmol^{-1}) is not reached. This drop of χ_MT at high temperature depends on the different nature of the spin-orbit coupling (SOC) on the Co(II) ion, being more abrupt in **3**, since a 1st order SOC, typical for octahedral cobalt(II) complexes is present, whereas **2** shows 2nd order SOC common on tetrahedral cobalt(II) complexes.[44,45] recent ref? Below 50 K, a drastic fall of χ_MT is observed until values of 0.54 and 0.41 cm^{3}Kmol^{-1} at 2 K for **2** and **3**. The unique presence of a SOC or zero-field splitting (zfs) will lead to a ~~lowest~~ value at 0 K equal to 1.125 cm^{3}Kmol^{-1} with g = 2. Therefore, in these complexes not only the depopulation of the higher energy Kramers doublets of the cobalt(II) ion occurs, also antiferromagnetic interactions are present between the cobalt(II) ions. Such interactions can be confirmed by the maximum of the χ_M product discerned at 2 K in **2**, and clearly observed in **3**.

The χ_MT value of **4** at 300 K is 4.30 cm^{3}Kmol^{-1}. This value is close to the corresponding of a high-spin manganese(II) ion with S = 5/2 (χ_MT = 4.375 cm^{3}Kmol^{-1} with g = 2). The χ_MT value remains constant up to 70 K and then decreases until 0.53 cm^{3}Kmol^{-1} at 2 K. A maximum of the χ_M product is observed at 5 K, suggesting antiferromagnetic interactions between the manganese(II) ions.

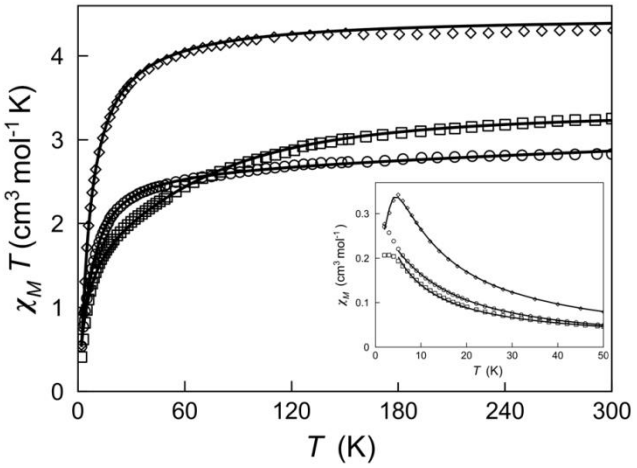

Figure 7. Plots of $\chi_M T$ *vs* T and χ_M *vs* T (inset) for **2** (○), **3** (□), and **4** (◇), in the range 2–300 K in 0.5 T applied field with the experimental fit (solid line).

Field-dependent magnetization plots for **2**–**4** at 2 K are given in Figure S10. The magnetization values at 5 T are 1.85, 1.80 and 3.17 Nβ for compounds **2**–**4**, respectively. These values are far below the saturation limit of 3 and 5 Nβ (for a cobalt(II) ion with S = 3/2 and g = 2 and a manganese(II) ion with S = 5/2 and g = 2). Therefore, these curves indicate the presence of weak antiferromagnetic interactions in all compounds and magnetic anisotropy in the cobalt(II) compounds.

Three types of magnetic pathways are present in compounds **2**–**4**, all of them via the O–P–O bridge adopting three very distorted *anti-syn* configuration. Furthermore, compound **4** has an additional magnetic pathway via the carboxylate ligand in an *anti-syn* configuration. Similar to the magnetic pathways on carboxylate ligands,[46] stronger antiferromagnetic behavior is expected for an *anti-anti* configuration than for a *syn-syn* configuration. However, weak (ferro)magnetic interactions are expected between the metal ions in *anti-syn* configuration. Overall, from magnetochemistry, we can conclude that predominant antiferromagnetic interactions are present in compounds **2**–**4**, as reported in similar systems.[47–49] The stronger antiferromagnetic interactions in **4**, as observed for the higher temperature of the maximum of the χ_M product, might be due to the presence of an additional antiferromagnetic pathway via carboxylate bridge as compared to **2** and **3**. Nevertheless, it is difficult to establish magnetostructural correlations due to the multiple magnetic exchange pathways and the different metal ions involved. Thus, theoretical calculations (see experimental section) were performed for compounds **2**–**4**.[50] Compounds **2** and **3** can be described as 2D magnetic systems linked by diamagnetic phosphoserine ligands, forming a 3D network (Figure S11), whereas compound **4** forms a 3D magnetic network (Figure S12). The efficiency to transmit the magnetic coupling by the long phosphoserine must be very weak or null, being this pathway neglected in this study. Thus, the only magnetic pathways considered for **2**–**4** are mediated by phosphate groups (J_{1-3}) and also by a carboxylate group (J_4) in **4**. The obtained results for the magnetic coupling constants and the intermetallic distances are shown in Table 4.[50] Although ferromagnetic and antiferromagnetic couplings were found, the last ones are predominant. Among of them, two couplings are responsible of the experimental magnetic behaviour in **2** and **4**, which allow describing our magnetic system as a square 2D network. However, in **3**, three magnetic couplings are significant constituting a Kagome 2D network. The stronger antiferromagnetic couplings in **3** are responsible for the maximum in χ_M, which is not observed in **2**.

Table 4. Calculated magnetic couplings (cm^{-1}) and intermetallic distances (Å) for **2**–**4**.

Compound	J_1	J_2	J_3	J_4	d_1	d_2	d_3	d_4
2	−0.48	+0.05	−0.46	−	5.141	5.202	5.769	−
3	+1.32	−1.42	−3.32	−	5.251	5.437	6.267	−
4	−0.48	−0.05	−0.18	−0.55	6.628	5.371	5.606	6.241

The simulation of the magnetic behaviour in such extended networks is not easy, even more when in **2** and **3**, the spin moments can be only considered as quantum spins and the cobalt(II) ion, through a SOC, presents a zfs that is larger than the magnetic coupling between the paramagnetic centers.[51] recent ref? Thus, the magnetic behaviour of **2** were simulated using a mean-field approach to include magnetic interactions between the anisotropic Co(II) ions with the following Hamiltonian: $H = D[S_z^2 + (1/3)S(S+1)] + \beta HgS$. The best-fit parameters obtained are: g = 2.39, D = 8.20 cm^{-1} and θ = − 3.13 cm^{-1} for **2** and g = 2.67, D = 85.58 cm^{-1} and θ = − 3.61 cm^{-1} for **3** (D = axial zfs parameter and θ = molecular interactions). The axial zfs parameter in **2** is one order of magnitude smaller than in **3**, which is reasonable because the different nature of the SOC in these compounds. This conclusion agrees with the D values calculated from CAS calculations (+ 15.7 and + 89.7 cm^{-1}). Fortunately, the S = 5/2 spin moment of the Mn(II) ion is large enough to consider it as a classical spin, *i.e.*, as a vector that can take any spatial direction. This approach is easy to implement and there is analytical laws to describe the alternating and regular square 2D network. Since theoretical values of J_1 and J_4 are very similar, we have used the analytical expression that relates χ_M with T/J to fit the experimental data. Our results (g = 2.02 and J = − 0.35 cm^{-1} for **4**), in agreement with the theoretical predictions, confirms the weak strength and the antiferromagnetic nature of the magnetic couplings.

Conclusions

Four coordination networks have been synthesized with the phosphoserine ligand. The crystal X-ray structure depends on the 3-d metal ion and the reaction conditions. All compounds

are formed by inorganic layers built up from MO_4 or MO_6 polyhedra and phosphonate groups, which are linked by the carboxylate groups of the phosphoserine ligand. These three-dimensional networks are stabilized by hydrogen bonding. Such interactions favour the proton transfer leading to moderate proton conductors. One remarkably feature is that the tetrahedral cobalt(II) network can be converted into the octahedral cobalt(II) network upon exposure at high relative humidity conditions. Antiferromagnetic interactions are present between the paramagnetic metal(II) ions due mainly to the *anti-syn* configuration of the phosphate bridges and also of the carboxylate bridge in **4**.

Future work is focused on the employ of a larger ligand to increase the pore size of the networks and to improve the conduction properties.

Conflicts of interest

There are no conflicts to declare.

Acknowledgements

This work was financially supported by the MCCC (CTQ2013-44844P and CTQ2016-75671-P), the Generalitat Valenciana (CTQ2013-44844-P) and "María de Maeztu" Excellence Unit by Mineco (MDM-2014-0538). M. V-C. acknowledges MINECO for a Juan de la Cierva research fellowship. We also acknowledge D. Vie (Universitat de València) for the TGA measurements. The work at UMA was funded by Spanish MINECO through MAT2013-41836-R and MAT2016-77648-R, which are co-funded by FEDER, and by Junta de Andalucía (P12-FQM-1656) projects.

Notes and references

1 S. Ma and H.-C. Zhou, *Chem. Comm.*, 2010, **46**, 44–53.
2 O. K. Farha and J. T. Hupp, *Acc. Chem. Res.*, 2010, **43**, 1166–1175.
3 J. Gascon, A. Corma, F. Kapteijn and F. X. Llabrés I Xamena, *ACS Catal.*, 2014, 4, 361–378.
4 M. D. Allendorf, C. A. Bauer, R. K. Bhakta and R. J. T. Houk, *Chem. Soc. Rev.*, 2009, **38**, 1330.
5 Y. Cui, Y. Yue, G. Qian and B. Chen, *Chem. Rev.*, 2012, 112, 1126–1162.
6 P. Horcajada, T. Chalati, C. Serre, B. Gillet, C. Sebrie, T. Baati, J. F. Eubank, D. Heurtaux, P. Clayette, C. Kreuz, J.-S. Chang, Y. K. Hwang, V. Marsaud, P.-N. Bories, L. Cynober, S. Gil, G. Ferey, P. Couvreur and R. Gref, *Nat. Mater.*, 2010, **9**, 172–178.
7 J. Della Rocca, D. Liu and W. Lin, *Acc. Chem. Res.*, 2011, **44**, 957–968.
8 C. Janiak, *Dalt. Trans.*, 2003, 2781–2804.
9 K. J. Gagnon, H. P. Perry and A. Clearfield, *Chem. Rev.*, 2012, 112, 1034–1054.
10 K. Maeda, *Microporous Mesoporous Mater.*, 2004, 73, 47–55.
11 G. K. H. Shimizu, R. Vaidhyanathan and J. M. Taylor, *Chem. Soc. Rev.*, 2009, **38**, 1430–1449.
12 A. Clearfield and K. D. Demadis, Eds., *Metal Phosphonate Chemistry: From synthesis to applications*, The Royal Society of Chemistry, London, 2012.
13 I. Imaz, M. Rubio-Martínez, J. An, I. Solé-Font, N. L. Rosi and D. Maspoch, *Chem. Commun.*, 2011, **47**, 7287.
14 S.-S. Bao and L.-M. Zheng, *Coord. Chem. Rev.*, 2016, **319**, 63–85.
15 Q. Chen, Z. Chang, W. C. Song, H. Song, H. Bin Song, T. L. Hu and X. H. Bu, *Angew. Chemie - Int. Ed.*, 2013, **52**, 11550–11553.
16 K. Klaus-Dieter, *Chem. Mater.*, 1996, **8**, 610–641.
17 2011.
18 I. Bryndal, B. Picur and T. Lis, *Zeitschrift fur Krist.*, 2004, **219**, 38–46.
19 R. He, X.-Y. Zhu, H.-H. Song and H.-T. Yu, *Chinese J. Inorg. Chem.*, 2013, **29**, 2085.
20 C. R. Groom, I. J. Bruno, M. P. Lightfoot and S. C. Ward, *Acta Crystallogr. Sect. B Struct. Sci. Cryst. Eng. Mater.*, 2016, **72**, 171–179.
21 A. D. Becke, *J. Chem. Phys.*, 1993, **98**, 5648.
22 M. J. Frisch, G. W. Trucks, H. B. Schlegel, G. E. Scuseria, M. A. Robb, J. R. Cheeseman, G. Scalmani, V. Barone, B. Mennucci, G. A. Petersson, H. Nakatsuji, M. Caricato, X. Li, H. P. Hratchian, A. F. Izmaylov, J. Bloino, G. Zheng, J. L. Sonnenberg, M. Hada, M. Ehara, K. Toyota, R. Fukuda, J. Hasegawa, M. Ishida, T. Nakajima, Y. Honda, O. Kitao, H. Nakai, T. Vreven, J. A. Montgomery, J. E. Peralta, F. Ogliaro, M. Bearpark, J. J. Heyd, E. Brothers, K. N. Kudin, V. N. Staroverov, R. Kobayashi, J. Normand, K. Raghavachari, A. Rendell, J. C. Burant, S. S. Iyengar, J. Tomasi, M. Cossi, N. Rega, J. M. Millam, M. Klene, J. E. Knox, J. B. Cross, V. Bakken, C. Adamo, J. Jaramillo, R. Gomperts, R. E. Stratmann., O. Yazyev, A. J. Austin, R. Cammi, C. Pomelli, J. W. Ochterski, R. L. Martin, K. Morokuma, V. G. Zakrzewski, G. A. Voth, P. Salvador, J. J. Dannenberg, S. Dapprich, A. D. Daniels, Ö. Farkas, J. B. Foresman, J. V. Ortiz, D. J. Cioslowski and D. J. Fox, 2009.
23 A. Schäfer, C. Huber and R. Ahlrichs, *J. Chem. Phys.*, 1994, **100**, 5829.
24 M. Cossi, N. Rega, G. Scalmani and V. Barone, *J. Comput. Chem.*, 2003, **24**, 669–681.
25 J. Tomasi, B. Mennucci and E. Cancès, *J. Mol. Struct. THEOCHEM*, 1999, **464**, 211–226.
26 E. Ruiz, A. Rodríguez-Fortea, J. Cano, S. Alvarez and P. Alemany, *J. Comput. Chem.*, 2003, **24**, 982–989.
27 E. Ruiz, J. Cano, S. Alvarez and P. Alemany, *J. Comput. Chem.*, 1999, **20**, 1391–1400.
28 F. Neese, *Wiley Interdiscip. Rev. Comput. Mol. Sci.*, 2012, 2, 73–78.
29 K. Eichkorn, F. Weigend, O. Treutler and R. Ahlrichs, *Theor. Chem. Acc.*, 1997, **97**, 119–124.
30 K. Eichkorn, O. Treutler, H. Öhm, M. Häser and R. Ahlrichs, *Chem. Phys. Lett.*, 1995, **240**, 283–289.
31 1995.
32
33 G. M. Sheldrick, *Acta Crystallogr. Sect. A Found. Crystallogr.*, 2008, **64**, 112–122.
34 A. Altomare, C. Cuocci, C. Giacovazzo, A. Moliterni, R. Rizzi, N. Corriero and A. Falcicchio, *J. Appl. Crystallogr.*, 2013, **46**, 1231–1235.
35 H. M. Rietveld, *J. Appl. Crystallogr.*, 1969, **2**, 65–71.
36 B. H. Toby, *J. Appl. Crystallogr.*, 2001, **34**, 210–213.

37 A. C. Larson and R. B. von Dreele, *Report No. LA-UR-2000, 86-748*, .

38 N. N. Greenwood and A. Earnshaw, *Chemistry of the Elements*, Oxford: Butterworth-Heinemann, Oxford, 2nd edn., 1997.

39 M. Bazaga-García, G. K. Angeli, K. E. Papathanasiou, I. R. Salcedo, P. Olivera-Pastor, E. R. Losilla, D. Choquesillo-Lazarte, G. B. Hix, A. Cabeza and K. D. Demadis, *Inorg. Chem.*, 2016, **55**, 7414–7424.

40 S. Kim, K. W. Dawson, B. S. Gelfand, J. M. Taylor and G. K. H. Shimizu, *J. Am. Chem. Soc.*, 2013, **135**, 963–966.

41 S. S. Bao, N. Z. Li, J. M. Taylor, Y. Shen, H. Kitagawa and L. M. Zheng, *Chem. Mater.*, 2015, **27**, 8116–8125.

42 M. Feyand, C. F. Seidler, C. Deiter, A. Rothkirch, A. Lieb, M. Wark and N. Stock, *Dalt. Trans.*, 2013, **42**, 8761.

43 P. Ramaswamy, N. E. Wong and G. K. Shimizu, *Chem Soc Rev*, 2014, **43**, 5913–5932.

44 R. L. Carlin, *Magnetochemistry*, Springer-Verlag, 1986.

45 O. Kahn, *Molecular Magnetism*, VCH Publishers, New York, 1993.

46 A. Rodríguez-Fortea, P. Alemany, S. Alvarez and E. Ruiz, *Chem. - A Eur. J.*, 2001, **7**, 627–637.

47 P. Yin, X. Wang, S. Gao and L. Zheng, *J. Solid State Chem.*, 2005, **178**, 1049–1053.

48 G. F. Han, H. Z. Luo, Q. Ye and R. G. Xiong, in *Zeitschrift fur Anorganische und Allgemeine Chemie*, 2008, vol. 634, pp. 1991–1995.

49 A. M. Chippindale, F. O. M. Gaslain, R. Cowley and A. V Powell, *J. Mater. Chem.*, 2001, **2**, 3172–3179.

50 J. Cano and Y. Journaux, in *Magnetism: Molecules to Materials V*, eds. J. S. Miller and M. Drillon, Wiley-VCH, Weinheim, 2005, pp. 189–222.

51 F. Lloret, M. Julve, J. Cano, R. Ruiz-García and E. Pardo, *Inorganica Chim. Acta*, 2008, **361**, 3432–3445.

